ADVANCED FUNCTIONAL MATERIALS
www.afm-journal.de

Amphiphilic Polymeric Nanocarriers with Luminescent Gold Nanoclusters for Concurrent Bioimaging and Controlled Drug Release

Dongyun Chen, Zhentao Luo, Najun Li, Jim Yang Lee, Jianping Xie,* and Jianmei Lu**

Multifunctional theranostic systems with good biocompatibility, strong clinical imaging capability, and target specificity are the desired features of future medicine. Here, the design of a theranostic nanocomposite capable of simultaneous targeting and imaging of the cancer cells is presented. It releases its drug payload by a controlled release mechanism. The nanocomposite contains luminescent gold nanocluster (*L*-AuNC) photostable and biocompatible diagnostic probes conjugated to a folic acid (FA)-modified pH-responsive amphiphilic polymeric system for controlled drug release. The nanocomposite uses a core-satellite structure to encapsulate hydrophobic drugs and releases the drug payload in mildly acidic endosomal/lysosomal compartments by the action of the pH-labile linkages in the polymer. In vivo studies show the selective accumulation of the FA-conjugated nanocomposite in tumor tissues by folate-receptor-mediated endocytosis. These findings demonstrate the potential of the nanocomposite as a nontoxic, folate-targeting, pH-responsive drug carrier that is useful for the early detection and therapy of folate-overexpressing cancerous cells.

1. Introduction

Cancer nanomedicine which combines medical imaging, molecular diagnosis, and targeted cell therapy in a single entity has drawn strong interest and much attention.[1–4] The most salient feature of cancer nanomedicine is the use of inorganic (e.g., magnetic nanoparticles (NPs), quantum dots (QDs), and gold NPs) and polymeric NPs (e.g., dendrimers and micelles) to provide functions and structures for cancer therapy which are not found in the bulk materials or discrete molecules.[5–8] Recent progress in nanotechnology has allowed inorganic and polymeric NPs to be synthesized with well-controlled properties and qualities.[9–12] The logical outgrowth from the current development of nanomedicine is the design and fabrication of multifunctional nanocomposites combining cancer cell imaging and therapy (theranostic nanocomposites).[13] Hence theranostic nanocomposites often contain two or more types of NPs with complementary functionalities. The functionalities, which are derived from the intrinsic properties of the components (e.g., optical properties of inorganic NPs and structural properties of polymeric NPs), are strategically combined into a common entity to synergize their interactions; and to deliver outcomes that would otherwise be difficult or impossible to accomplish in single-component NP systems.

This study demonstrates our effort in producing a novel theranostic nanocomposite by a facile approach, which is capable of cancer cell imaging, targeted drug delivery and controlled drug release. The theranostic nanocomposite was formed by the self-assembly of an ultrasmall non-toxic luminescent imaging agent, a cancer cell targeting agent, a hydrophobic drug; and a pH-responsive amphiphilic polymeric nanocarrier into the interesting core-satellites structure shown in **Scheme 1**. The luminescent gold nanoclusters (hereafter referred to as *L*-AuNCs) and an amphiphilic polymeric system with pH-labile linkages are the two key elements in the design of the theranostic nanocomposite.

Highly luminescent AuNCs were the imaging agent in the design. AuNCs are ultrasmall particles with a core size below 2 nm and contain 150 Au atoms or less.[14,15] Due to the strong quantum confinement of free electrons in this size range, AuNCs exhibit some unique optical properties such as strong luminescence.[16–18] Unlike the common luminescent imaging agents (e.g., organic dyes and QDs) where applicability may be limited by low photostability (e.g.,organic dyes) or toxicity considerations (e.g., QDs of heavy metals), the excellent photostability, good biocompatibility, and low toxicity *L*-AuNCs are the desired features of next generation imaging probes.[19–22] An added advantage of *L*-AuNCs is their very small hydrodynamic size (<3 nm, comparable to most organic dyes). Particles in this size range are known to show very efficient renal clearance, which is an important consideration for in vivo applications.[23–25]

Dr. D. Chen, Prof. N. Li, Prof. J. Lu
College of Chemistry
Chemical Engineering and Materials Science
Soochow University
Suzhou, 215123, China
E-mail: lujm@suda.edu.cn
Z. Luo, Prof. J. Y. Lee, Prof. J. Xie
Department of Chemical & Biomolecular Engineering
Faculty of Engineering
National University of Singapore
Singapore, 117576
E-mail: cheleejy@nus.edu.sg; chexiej@nus.edu.sg

DOI: 10.1002/adfm.201300411

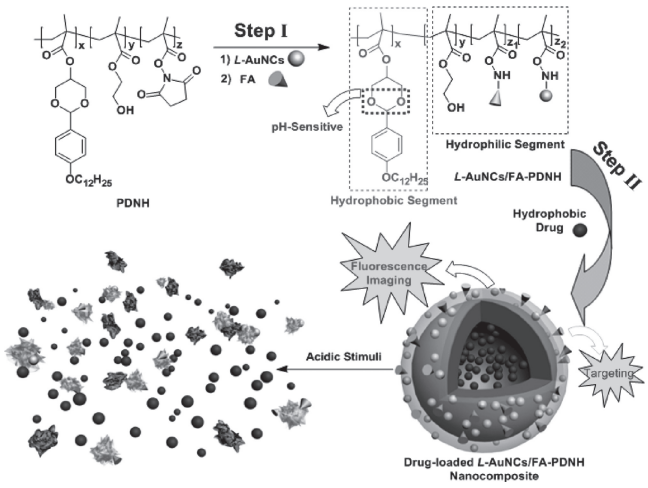

Scheme 1. Schematic illustration of the fabrication of theranostic *L*-AuNCs/FA-PDNH nanocomposite.

Amphiphilic polymeric nanocarriers are an ideal platform for drug delivery because of their highly customizable structure and proven drug loading performance.[26–28] They also have other useful features such as improved preferential accumulation in tumors via the enhanced permeability and retention (EPR) effect, prolonged circulation time, improved drug bioavailability, and few side effects.[29–34] Biodegradable nanocarriers which are pH, temperature, or enzymatic reaction responsive have been used to release their drug payloads within the affected cells or organs.[35–38] For example, a smart and efficient drug-release system may be constructed by incorporating pH-labile linkages into the polymeric nanocarriers. The expeditious hydrolysis of the nanocarriers in the acidic environment (pH 5-6) of endosomes or lysosomes could then trigger the controlled release of the drug payloads within the targeted cells.

The integration of *L*-AuNCs and pH-responsive amphiphilic polymeric nanocarriers into a theranostic nanocomposite was accomplished in this study via the self-assembly of the functional components. The nanocomposite fabricated as such displayed a core-satellites nanostructure with the polymeric nanocarrier as the core and *L*-AuNCs as the satellites in the shell (Scheme 1). The core-satellites nanocomposite was able to specifically target the cancer cells and unload the therapeutic drug effectively within. The drug delivery process could be continuously monitored by the luminescence of the co-delivered imaging probes (*L*-AuNCs).

2. Results and Discussion

The preparation of the theranostic nanocomposite as shown in Scheme 1 involved two steps. In the first step the bioimaging probe (*L*-AuNCs) and the targeting ligand (folic acid, FA) were tethered to the amphiphilic copolymer (poly(DBAM-*co*-NAS-*co*-HEMA) (PDNH)) to form *L*-AuNCs/FA-modified PDNH (or *L*-AuNCs/FA-PDNH) nanocomposite. Prior to that the *L*-AuNCs and amphiphilic copolymer PDNH were synthesized and purified according to a previous procedure of ours.[39,40] The AuNCs were approximately 1 nm (**Figure 1**a) in size and had an intense orange luminescence (λ_{em} = 610 nm, Figure 1b, solid line). The *L*-AuNCs were capped by glutathione (GSH, γ-Glu-Cys-Gly), a water-soluble natural tripeptide, for biocompatibility.[41] The affinity between the thiol group of GSH (from the cysteine residue) and Au atoms provided a strong protection for the ultrafine AuNCs. The amine groups from *L*-AuNCs (from GSH) and FA could readily be conjugated to the activated esters of PDNH (Scheme 1) via a common amine coupling method, thereby finalizing the preparation of *L*-AuNCs/FA-PDNH nanocomposite.

The second step was the self-assembly of *L*-AuNCs/FA-PDNH with the hydrophobic anticancer drug, paclitaxel (PTX), to form a core-satellites nanocomposite in water (Scheme 1). The optimal monomer feed ratio [DBAM]:[NAS-HEMA] for the formation of amphiphilic PDNH copolymer had earlier been determined to be 1:6. See Table S1 (Supporting Information) for a detailed listing of the polydispersity index, molecular weight, and the assembly characteristics under different feed ratios. A theoretical study suggests that the self-assembly of amphiphilic copolymers starts from unimers to overlapped brushes.[42] Growth of the polymeric particles stopped when the overlapping brushes had grown to a critical size. As shown in Scheme S1 (Supporting Information), the self-assembly of PDNH continued until a critical size was reached (stage II). Thereafter the aggregation of unimers was slower than the exchange between unimers; and the latter process dominated in the further growth of the polymeric particles to the final

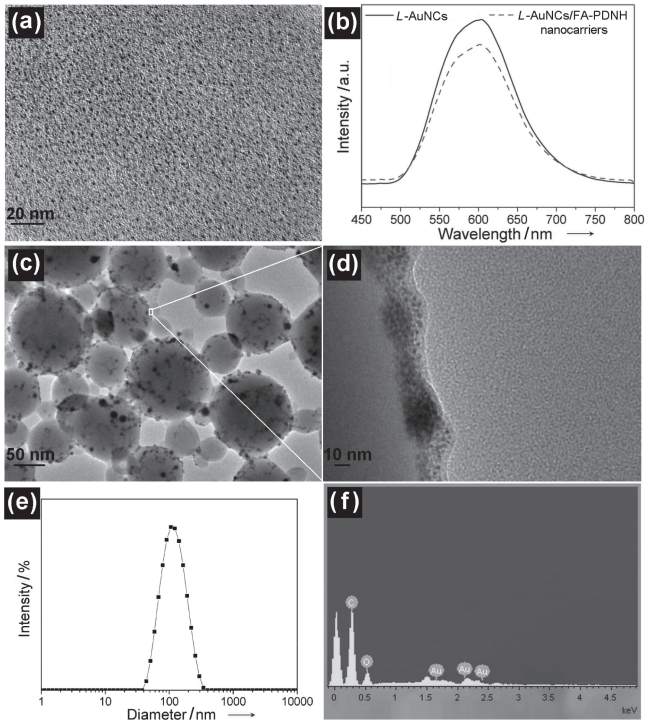

Figure 1. a) TEM image of the as-prepared *L*-AuNCs. b) Luminescence spectra of *L*-AuNCs and *L*-AuNCs/FA-PDNH nanocomposite. c) TEM, d) HRTEM, e) DLS, and f) EDS analyses of the as-fabricated *L*-AuNCs/FA-PDNH nanocomposite.

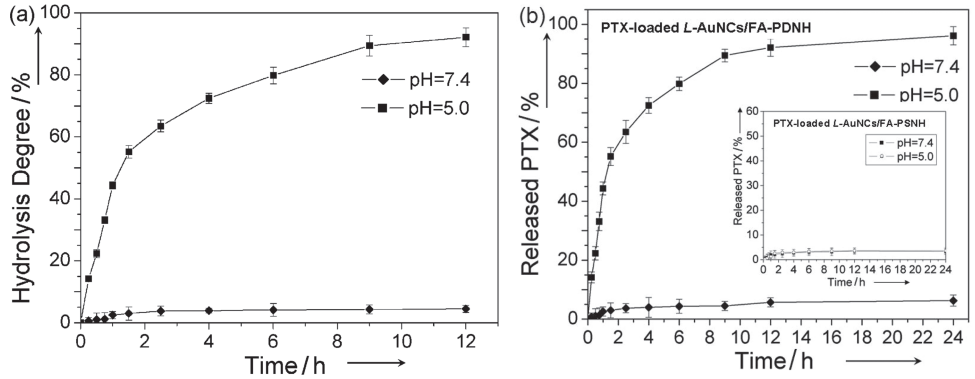

Figure 2. a) Extent of hydrolytic decomposition of the copolymer and b) PTX release profiles of PTX-loaded *L*-AuNCs/FA-P**D**NH and *L*-AuNCs/FA-P**S**NH (inset) nanocomposites in 12 and 24 h, respectively, at pH 7.4 (diamond) and pH 5.0 (square).

equilibrium size (stage III, ≈120 nm). The core of the polymeric particles is likely to contain additional polymer chains which contributed to the size and structural stability of the *L*-AuNCs/FA-PDNH nanocomposite. The self-assembly of *L*-AuNCs and FA-modified PDNH was similar to the self-assembly of PDNH (see Figure S1 (Supporting Information) for the corresponding TEM image). Hence the incorporation of AuNCs and FA into PDNH did not affect the self-assembly characteristics of the amphiphilic copolymer. This was because the small size (≈1 nm) of the AuNCs could keep the disruption to the copolymer structure at a minimum. Figure 1b shows photoemission spectrum of the as-fabricated nanocomposite (Figure 1b, dotted line) which is nearly identical to that of *L*-AuNCs (solid line). The average diameter measured from a representative transmission electron microscopy (TEM) image (Figure 1c) was ≈120 nm. The TEM image also revealed the core-satellites structure of the nanocomposite–where a core of polymeric nanocarrier containing the hydrophobic cancer drug PTX was decorated with satellites of *L*-AuNCs (Scheme 1). The high-resolution TEM (HRTEM) image in Figure 1d shows that *L*-AuNCs (black dots) were large in number and well dispersed in the surface region of the polymeric nanocarrier core (lighter colored). Dynamic light scattering (DLS) measured a hydrodynamic diameter of 120 ± 30 nm for the as-fabricated nanocomposite (Figure 1e). The relatively small size of the nanocomposite (<200 nm) was favorable for a good drug delivery performance based on minimal renal excretion, low levels of reticuloendothelia system (RES) uptake, and improved passive tumor targeting via the EPR effect.[43] The nanocomposite composition as determined by the energy dispersive X-ray spectroscopy (EDS, Figure 1f) of a single nanocomposite particle also confirmed the confinement of *L*-AuNCs to the surface region of the polymeric nanocarrier.

The amount of PTX in the nanocomposite was estimated by the characteristic absorption of PTX at 227 nm to be ≈82 ± 3 μg-drug per mg-nanocomposite. The as-fabricated nanocomposite showed good stability in the PBS buffer and in blood serum at the physiological pH (7.4). There was no significant drug release from the PTX-loaded *L*-AuNCs/FA-PDNH nanocomposite in both media for two weeks (Figure S2, Supporting Information). The rate of hydrolysis and consequently the rate of drug release from the nanocomposite were strongly pH dependent. **Figure 2**a shows that the hydrolysis of the polymeric nanocarrier over a 12 h period was negligible at the physiological pH of 7.4, indicating that the nanocomposite was stable in the physiological environment. On the contrary, very fast hydrolysis was detected at pH 5.0 resulting in approximately 90% nanocomposite decomposition in 12 h. Figure 2b shows that the release of PTX from the *L*-AuNCs/FA-P**D**NH nanocomposite closely mirrored the decomposition profile of the polymeric carrier. Consequently while the release of PTX was negligible over 24 h at pH 7.4, most of the drug was released within 12 h at the weakly acidic pH of 5.0, and approximately 95% of the drug payload would be gone in 24 h. On the contrary, the release profile of PTX from the *L*-AuNCs/FA-PSNH nanocomposite [PSNH is the amphiphilic polymer poly(SMA-*co*-NAS-*co*-HEA) where there is no pH-labile linkage; SMA: stearyl methacrylate] at pH 5.0 and 7.4 (Figure 2b inset) was very similar to that of *L*-AuNCs/FA-PDNH nanocomposite at pH 7.4 (Figure 2b, diamond). These results are further indication that the pH-labile linkages in PDNH were responsible for the controlled release of PTX from the *L*-AuNCs/FA-PDNH nanocomposite. The strongly pH-dependent release profile of the nanocomposite is an ideal platform for targeted drug delivery since drug release is inhibited during systemic circulation at the physiological pH of 7.4. The drug is released only in the acidic environment of the affected cells.

The efficacy of the nanocomposite for cancer treatment was evaluated using the human hepatoma BEL-7402 cell line (7402 cells). We treated the 7402 cell culture with different concentrations of PTX-free *L*-AuNCs/FA-P**D**NH nanocomposite, PTX-loaded *L*-AuNCs/FA-P**D**NH nanocomposite, and PTX-loaded *L*-AuNCs/FA-P**S**NH nanocomposite. The viability of the cells after 24 h was measured by the sulforhodamine B (SRB) assay. The results in **Figure 3** (circle) show that PTX-free *L*-AuNCs/FA-PDNH nanocomposite had very low cytotoxicity (cell viability > 95% after 24 h) even at a high dosage of 0.6 mg mL^{-1}. The data could also be taken to suggest the good biocompatibility of the nanocomposite. Similarly, when the 7402 cells were incubated with PTX-loaded *L*-AuNCs/FA-P**S**NH nanocomposite (Figure 3, triangle) for 24 h, cell viability was also high (≈85%) and changed very little with increasing nanocomposite

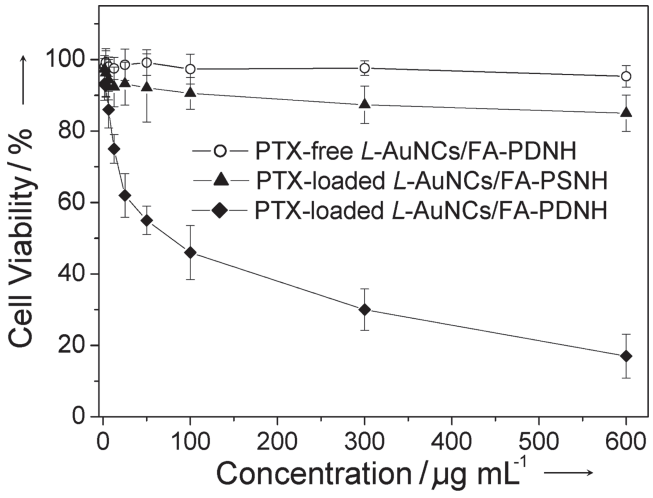

Figure 3. Viability of 7402 cells after incubation with PTX-free *L*-AuNCs/FA-PDNH nanocomposite (circle), PTX-loaded *L*-AuNCs/FA-PSNH nanocomposite (triangle), and PTX-loaded *L*-AuNCs/FA-PDNH nanocomposite (diamond) for 24 h.

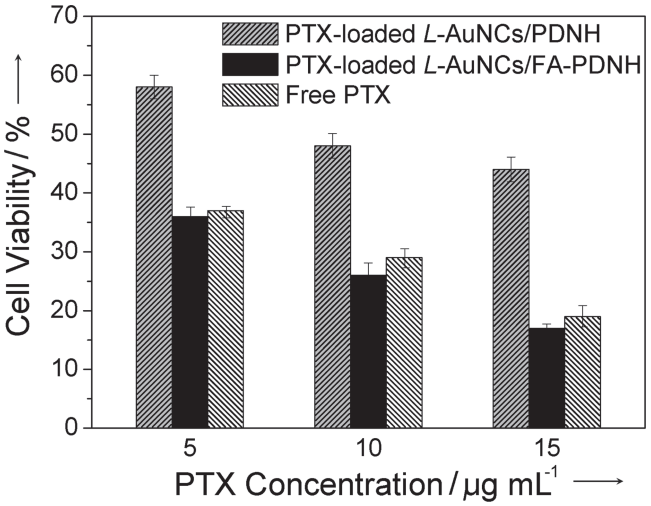

Figure 4. Viability of KB cells after incubation with PTX-loaded *L*-AuNCs/FA-PDNH nanocomposite, PTX-loaded *L*-AuNCs/PDNH nanocomposite, and free PTX at different PTX concentrations (5, 10, and 15 μg mL^{-1}) for 24 h.

concentration. This is an anticipated outcome since the PTX-loaded *L*-AuNCs/FA-P**S**NH nanocomposite, without a pH-labile linkage, was stable in the acidic (pH 5–6) endosomal or lysosomal compartments of the cancer cells. Consequently very little drug payload could be released from the nanocomposite. The situation was markedly different for 7402 cells incubated with the PTX-loaded *L*-AuNCs/FA-PDNH nanocomposite (Figure 3, diamond). Here cell viability decreased very rapidly with time resulting in a ≈23% survival after 4 h of incubation. This is an indication of the efficient uptake of the as-fabricated pH-responsive nanocomposite (PTX-loaded *L*-AuNCs/FA-PDNH nanocomposite) by the cancer cells and the successful release of the drug payload inside the cells.

The targeting effectiveness of the FA ligands in the nanocomposite against cancer cells was evaluated using a cancer cell line with an over-expressed folate receptor (FR, e.g., KB cells). The KB cells were treated with PTX-loaded *L*-AuNCs/FA-PDNH nanocomposite, PTX-loaded *L*-AuNCs/PDNH nanocomposite (without the targeting FA ligands), and free PTX in different concentrations for 24 h. As expected, the viability of the KB cells depended strongly on the PTX dosage (**Figure 4**). Furthermore it was observed that the PTX-loaded *L*-AuNCs/FA-PDNH nanocomposite displayed the same cytotoxicity against the KB cells as free PTX, at levels much higher than that of PTX-loaded *L*-AuNCs/PDNH nanocomposite without the FA ligand (Figure 4). The considerable cytotoxicity difference between FA-conjugated (*L*-AuNCs/FA-PDNH) and non-FA-conjugated (*L*-AuNCs/PDNH) nanocomposites simply confirmed the high selectivity of the FA ligands for the KB cells. A nanocomposite with FA ligands was able to specifically target the KB cells and be transported into the cell interior via the direct folate-receptor-mediated endocytosis pathway. The release of the PTX payload in the cytoplasm due to the low local pH environment therefore gave rise to cytotoxicity against the KB cells which was nearly as good as that of free PTX.

The different uptake behavior of FA-conjugated and non-FA-conjugated nanocomposites was also confirmed by confocal laser scanning microscopy (CLSM). Here the strong luminescence of the *L*-AuNCs in the nanocomposite designs provided an in-situ means to monitor the cellular uptake of the nanocomposite. In brief the KB cells were treated with FA-conjugated (*L*-AuNCs/FA-PDNH) and non-FA-conjugated (*L*-AuNCs/PDNH) nanocomposites at the same PTX concentration of 15 μg mL^{-1} and luminescence was monitored over a period of 3 h. Very little cellular uptake occurred in the first 0.5 h for the non-FA-conjugated (**Figure 5**a1) and FA-conjugated nanocomposites (Figure 5b1). The orange luminescence from the nanocomposite (from *L*-AuNCs) was faint in the cytoplasm of the cancer cells. The internalization of FA-conjugated and non-FA-conjugated nanocomposites by the cancer cells via endocytosis was nonetheless demonstrated, and the nanocomposites resided mainly in the cytoplasm. A significant difference in cellular uptake between the two nanocomposites occurred after 3 h of incubation, where stronger orange luminescence was emitted from cancer cells treated with the FA-conjugated nanocomposite (*L*-AuNCs/FA-PDNH, Figure 5b2) than cancer cells treated with the non-FA-conjugated nanocomposite (*L*-AuNCs/PDNH, Figure 5a2). The difference simply reflected the targeting effectiveness of the FA ligands in the FA-conjugated nanocomposite. The 7402 cells without over-expressed folate receptors (Figure 5c2) also luminesced weakly compared with the KB cells after 3 h of incubation with the PTX-loaded *L*-AuNCs/FA-PDNH nanocomposite (Figure 5b2); another demonstration of the importance of the FA ligands in the nanocomposite design for targeting specific cancer cells. The higher drug efficacy of the FA-conjugated nanocomposite in the KB cells could then be unambiguously attributed to the enhanced cellular uptake of the nanocomposite via the folate-receptor-mediated endocytosis pathway.

The encouraging results from the in vitro study promoted an in vivo trial to evaluate the potential of the nanocomposite for clinical use. A dose-tolerance study was first carried out using healthy Balb/c mice. The mice were intravenously injected with free PTX to concentrations of 30, 40, or

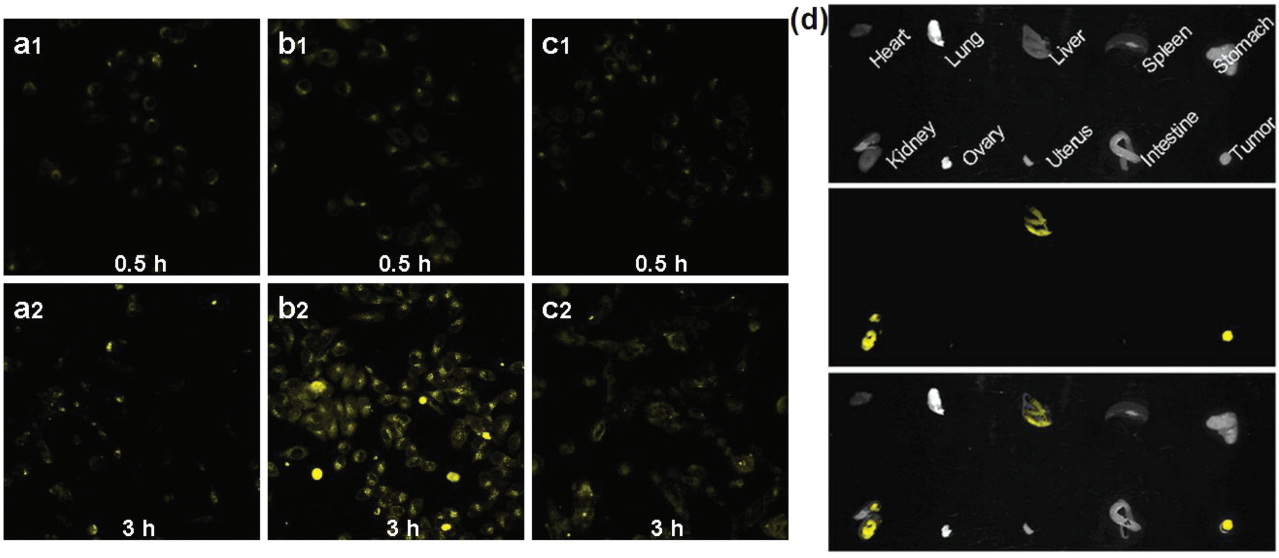

Figure 5. Representative CLSM images of KB cells incubated with a) non-FA-conjugated nanocomposite (*L*-AuNCs/PDNH) and b) FA-conjugated nanocomposite (*L*-AuNCs/FA-PDNH) for 0.5 h (upper row) and 3 h (lower row). c) CLSM images of 7402 cells incubated with the FA-conjugated nanocomposite for 0.5 h (upper row) and 3 h (lower row). d) Representative ex vivo white light images (top), luminescence images (middle) and overlaid images (bottom) of the dissected organs of sacrificed mice bearing the HeLa tumor at 24-h after the intravenous injection of FA-conjugated nanocomposite (*L*-AuNCs/FA-PDNH).

50 mg-PTX per kg-body weight; or with PTX-loaded *L*-AuNCs/FA-PDNH nanocomposite to effective PTX concentrations of 40, 60, and 80 mg-PTX per kg-body weight. Normal saline solution was used as the control. The mice treated with 40 mg of free PTX showed obvious weight loss in two weeks, and died immediately if 50 mg of free PTX was intravenously administrated. On the contrary, even at the highest equivalent dose of 80 mg PTX, the mice treated with PTX-loaded *L*-AuNCs/FA-PDNH nanocomposite showed no weight loss and were alive for two weeks. These in vivo results confirm the toxicity of PTX-loaded *L*-AuNCs/FA-PDNH nanocomposite is lower than that of free PTX at equivalent PTX doses. Figure S3 (Supporting Information) compares between the in vivo pharmacokinetics of *L*-AuNCs/FA-PDNH nanocomposite and free PTX. The gradual decrease of PTX concentration from the PTX-loaded *L*-AuNCs/FA-PDNH nanocomposite over 24 h after injection is in strong contrast with the rapid clearing of injected free PTX (the control group) from the body within the first two hours after injection. The long systemic circulation and slow elimination from blood are promising for a high clinical efficacy. The good stability of PTX-loaded *L*-AuNCs/FA-PDNH nanocomposite in media and in blood could be attributed to the combination of structural stability and a relatively small size (<200 nm). In addition, the hydrophilic segments in the polymer carrier are mostly pHEMA [poly(2-hydroxyethyl methacrylate)], which is known to be stealthy and biocompatible.[44] The *L*-AuNCs were also coated with a naturally occurring peptide, GSH, which has the ability to minimize non-specific protein adsorption in blood.[23,25,45] The observed good stability of the as-fabricated nanocomposite in blood circulation is not totally unexpected in view of its biocompatibility and stealthy coating.

Female athymic nude mice bearing the HeLa (FR-expressing) tumors with a tumor size of ≈0.5 cm (after 3 weeks post-inoculation of 1×10^6 cells on the right foreleg) were then selected as the animal model. The mice were intravenously injected with 4 mg-PTX per kg-body weight of free PTX or PTX-loaded *L*-AuNCs/FA-PDNH nanocomposite. The mice were then sacrificed at 0.5, 2, 6, 12, and 24 h after drug administration, and the concentrations of PTX in various tissues at different times were calculated. The PTX distributions from free PTX and PTX-loaded *L*-AuNCs/FA-PDNH nanocomposite in different tissues are summarized in Table S2 (Supporting Information). The PTX concentration from injected PTX-loaded *L*-AuNCs/FA-PDNH nanocomposite was lower than that of injected free PTX in normal tissues except at the tumor sites. These data suggest that PTX-loaded *L*-AuNCs/FA-PDNH nanocomposite is lower in toxicity and has better efficacy than free PTX.

The tumor targeting capability of the nanocomposite was evaluated by injecting FA-conjugated nanocomposite (*L*-AuNCs/FA-PDNH) or non-FA-conjugated nanocomposite (*L*-AuNCs/PDNH) intravenously into the mice, and monitoring the distribution of the nanocomposite by its luminescence over the course of one day. As shown in Figure 5d and **Figure 6**, a strong luminescence was emitted from the tumor sites a day after the injection of the FA-conjugated nanocomposite. On the contrary, no luminescence was detected in the tumor of the mouse injected with the non-FA-conjugated nanocomposite (data not shown). Figure 5d (the middle panel) also shows that luminescence was localized at the tumor rather than in other major organs (e.g., kidney and liver). The high targeting efficiency of the nanocomposite (from the FA ligand) against the FR-expressing tumor, and the enhanced uptake of the nanocomposite in the tumor tissues via the direct folate-receptor-mediated endocytosis pathway, was once again demonstrated. In addition, Figure 6 shows that the nanocomposite was rarely

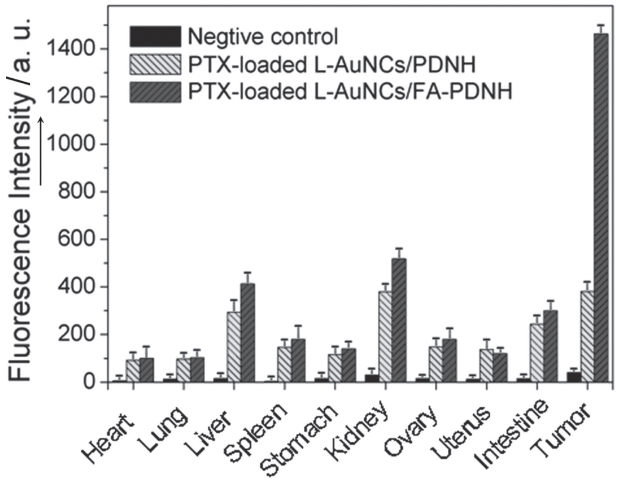

Figure 6. Luminescence intensities of the dissected organs of sacrificed mice bearing the HeLa tumor at 24-h after the intravenous injection of FA-conjugated nanocomposite (*L*-AuNCs/FA-PDNH).

found in most of the organs, indicating that the nanocomposite had sufficient transit time in systemic circulation for the targeting of the tumor. Some deposition of the nanocomposite was however detected in kidney and liver due to the special binding affinity and metabolic processes in these organs. The localization of the nanocomposite (*L*-AuNCs/FA-PDNH) in the FR-expressing tumor tissues also indicated negligible uptake of the nanocomposite by macrophages.

3. Conclusions

In conclusion, we have designed and built a multifunctional nanocomposite that provided selective targeting, in-situ imaging and anticancer therapy functionalities by encapsulating a hydrophobic drug in *L*-AuNCs conjugated pH-labile targeting polymeric carriers. The nanocomposite, in the form of *L*-AuNCs/FA-PDNH, was water-stable and biocompatible; and could release its drug payload at a weakly acidic pathological site via polymer degradation processes, while the *L*-AuNCs provided positioning information and the hydrophobic drug provided the therapeutic action at the targeted cells. Both in vitro and in vivo studies confirmed the efficacy of this theranostic composite for cancer cell targeting and treatment.

4. Experimental Section

Chemicals: *p*-Hydroxybenzaldehyde, benzyl chloride, 1-bromododecane, *p*-toluenesulfonic acid (PTSA), sodium methoxide and glycerol were purchased from Shanghai Chemical Reagent Co. Ltd. and used without further purification. Dodecyl 2-methylacrylate, L-glutathione reduced, stearyl methacrylate (SMA) and N-succinimidyl methacrylate (NAS) were supplied by Sigma-Aldrich. Hydrogen tetrachloroauratetrihydrate ($HAuCl_4 \cdot 3H_2O$) was provided by Alfa Aesar. 2-Hydroxyethyl methacrylate (HEMA) was distilled under vacuum and stored at –15 °C under an inert gas atmosphere. Other reagents were commercially available and used as received.

Synthesis of 4-n-Dodecyloxybenzalacetal Monomer (DBAM): 4-*n*-dodecyloxybenzaldehyde (DBD) was synthesized according to the following procedure. 1-bromododecane (29.9 g, 120 mmol) was added dropwise to an acetone solution (150 mL) containing anhydrous potassium carbonate (20.7 g, 150 mmol) and *p*-hydroxybenzaldehyde (12.2 g, 100 mmol). After heating under reflux and vigorous stirring for 14 h, the crude product was purified by column chromatography (ethyl acetate-petroleum ether, 1:10).Then, DBD (8.7 g, 30 mmol) was reacted with glycerol (2.76 g, 30 mmol) in toluene (50 mL) using PTSA (0.5 g) as the catalyst. The solution was refluxed for 14 h and the water formed in the dehydrogenation reaction was removed by an oil-water separator. The mixture was then concentrated by reduced pressure distillation and washed with potassium carbonate solution (1%, 80 mL) to remove the acid catalyst and residual glycerol. The precipitate was collected and purified by column chromatography (ethyl acetate-petroleum ether, 1:2) to obtain 4-n-dodecyloxybenzalacetal (DBA).

Methacryloyl chloride (2.3 g, 22 mmol) was added slowly to an anhydrous tetrahydrofuran (20 mL) solution of triethylamine (4.5 g, 44 mmol) and DBA (4.0 g, 11 mmol) and cooled to 0 °C in an ice-water bath. After continuous stirring for another 12 h at room temperature, the mixture was filtered to remove insoluble byproducts. The filtrate obtained as such was concentrated and purified by column chromatography (ethyl acetate-petroleum ether, 1:8). Anal. Calcd. for $C_{26}H_{40}O_5$: C 72.19, H 9.32, O 18.49; found: C 72.30, H 9.28, O 18.42. ^{1}H NMR (400 MHz, $CDCl_3$, δ): 7.41 (d, J = 8.39 Hz, 2H, C_6H_4), 6.89 (d, J = 8.41 Hz, 2H, C_6H_4), 6.30 (s, 1H, CCH_2), 5.65 (s, 1H, CCH_2), 5.52 (s, 1H, C_6H_4CH), 4.75 (s, 1H, CHO), 4.31 (d, J = 12.88 Hz, 2H, $CHCH_2O$), 4.18 (d, J = 12.92 Hz, 2H, $CHCH_2O$), 3.95 (t, J = 6.59 Hz, 2H, $C_6H_4OCH_2$), 2.01 (s, 3H, CH_3), 1.81-1.72 (m, 2H, CH_2CH_2O), 1.49-1.38 (m, 2H, $CH_2CH_2CH_2O$), 1.26 (m, 16H, CH_2), 0.88 (t, J = 6.68 Hz, 3H, CH_2CH_3). ^{13}C NMR (75 MHz, $CDCl_3$, δ): 167.45 (s, 1C, COO), 159.95 (s, 1C, C), 136.28 (s, 1C, CCH_3), 132.25 (s, 1C, C), 127.57 (s, 2C, CH), 126.50 (s, 1C, CCH_2), 114.52 (s, 2C, CH), 74.21 (s, 1C, CH_2CO), 69.25 (s, 2C, CH_2CO), 68.28 (s, 1C, $CHCH_2O$), 32.16 (s, 1C, $CH_2CH_2CH_3$), 29.28-29.88 (m, 7C, CH_2), 26.24 (s, 1C, $CH_2CH_2CH_2O$), 22.94 (s, 1C, CH_2CH_3), 18.52 (s, 1C, CCH_3), 14.39 (s, 1C, CH_3).

Synthesis of Amphiphilic Copolymer Poly(DBAM-co-NAS-co-HEMA): The amphiphilic copolymer poly(DBAM-*co*-NAS-*co*-HEMA) (PDNH) was prepared by free radical copolymerization of DBAM, NAS and HEMA in cyclohexanone using AIBN initiator. Typically, AIBN (5.0 mg) was added to a cyclohexanone solution (2 mL) with DBAM (150 mg), HEMA (306 mg) and NAS (60 mg) in a test tube. The test tube was sealed and cycled between vacuum and nitrogen thrice. After 5 h reaction in an oil bath at 60 °C, the mixture was concentrated in a rotary evaporator and washed with a large quantity of anhydrous ether. The precipitate was recovered by centrifugation, dried under vacuum and stored in a desiccator for further use. In addition, poly(SMA-*co*-NAS-*co*-HEA) (PSNH) was synthesized following a similar procedure and used as the control.^{1}H NMR (400 MHz, DMSO-d_6, δ): 7.44 (C_6H_4), 6.94 (C_6H_4), 4.21-3.76 ($COOCH_2CH_2$, $CHCH_2O$ and $C_6H_4OCH_2$), 0.89-1.77 ($OC_{12}H_{25}$).

Synthesis of Luminescent Gold Nanoclusters (L-AuNCs): The synthesis and purification of *L-AuNCs* followed an earlier procedure of ours. In a typical synthesis, freshly prepared aqueous solutions of $HAuCl_4$ (20 mM, 1.0 mL) and GSH (100 mM, 0.30 mL) were mixed with of ultrapure water (8.7 mL) at 25 °C for 1 min. The reaction mixture was then heated to 70 °C under gentle stirring (500 rpm) for 24 h. The resultant aqueous solution of strongly orange-emitting AuNCs was purified using size-exclusion chromatography (Cat. No. 17-0851-01, GE Healthcare) and freeze-dried for further use.

Conjugation of L-AuNCs and Folic Acid with Poly(DBAM-co-NAS-co-HEMA): 3 mL of *L*-AuNCs (2 mM) in anhydrous dimethyl sulfoxide (DMSO) was added to PDNH (2 mL) in DMSO, and the reaction mixture was stirred overnight at room temperature. The mixture was then added to an excess of anhydrous ether to precipitate the polymer. The as-prepared *L*-AuNCs/PDNH was freeze-dried and stored in the dark at 4 °C. The folic acid was conjugated to *L*-AuNCs/PDNH following the same procedure described previously for the preparation of *L*-AuNCs/FA-PDNH.

Drug Loading and Release: For the evaluation of the drug loading and release properties of the nanocomposite, a hydrophobic anti-cancer

drug, PTX, was first loaded into *L*-AuNCs/FA-PDNH nanocomposite by adding PTX (50 μL, 10 mg mL^{-1}) to the as-prepared *L*-AuNCs/FA-PDNH in tetrahydrofuran (0.6 mL), followed by the slow addition of 5 mL of phosphate buffered saline (PBS, pH = 7.4). The solution was then shaken overnight to completely evaporate the tetrahydrofuran. The drug release rate was measured by dispersing the PTX-loaded *L*-AuNCs/FA-PDNH nanocomposite in a PBS buffer at a pH of interest, and the solution was shaken in a water bath at 37 °C. The drug concentration was calculated by optical density measurements at 227 nm.

Cell Culture: Human hepatoma 7402 and human KB cell lines (obtained from Shanghai Cell Institute Country Cell Bank, China) were cultured as a monolayer in RPMI-1640 medium supplemented with 10% heat-inactive fetal bovine serum. Culture was maintained in a humidified incubator (5% CO_2 in air by volume) at 37 °C.

In Vitro Cytotoxicity Study: The sulforhodamine B (SRB) assay was used to evaluate the cytotoxicity of the nanocomposite. In brief, the hepatoma 7402 cells were placed in a 96-well plate with seeding cells of ≈1.3×10^4 per well. Four duplicate wells were set-up for each sample. The culture medium was then replaced with the medium containing the *L*-AuNCs/FA-PDNH nanocomposite in different concentrations, and the culture was maintained at standard culture condition of 37 °C for 24 h. The medium was decanted, followed by the addition of 10 w/v% trichloroacetic acid (100 μL) in Hank's balanced salt solution. The culture was allowed to incubate at 4 °C for 1 h. The stationary liquid was then discarded, and the cells were washed copiously with deionized water for five times, followed by air drying and subsequent staining with 0.4 w/v% SRB solution (100 μL per well) for 30 min at room temperature. The SRB solution was removed and the cells were washed with 0.1% acetic acid solution for five times. The bound SRB dyes was then solubilized in a Tris-base solution (150 μL, 10 mM, pH = 10.5). The optical density at 531 nm was used to determine the cell viability.

Cellular Uptake of Drug-Loaded L-AuNCs/FA-PDNH Nanocomposite: Hepatoma 7402 cellswere seeded in a 96-well plate with ≈1.3×10^4 cells per well. The cell culture was incubated overnight in a humidified incubator at 37 °C. The nanocomposite dispersion was prepared in RPMI-1640 medium and the concentration of *L*-AuNCs/FA-PDNH nanocomposite was adjusted to ≈10 μg mL^{-1}. The nanocomposite was then added to the cell culture, and the culture was incubated for 30 min under standard culture condition. The cell culture was washed three times with PBS buffer, and then subjected to fluorescence microscopy examination. The fluorescence images were acquired by an Olympus IX-51 inverted microscopeequipped with 100 W mercury-xenon arc lamp excitation light source and high speed CCD camera.

In Vivo Pharmacokinetic Studies: Balb/c mice were intravenously injected with the *L*-AuNCs/FA-PDNH nanocomposite and free PTX at an equivalent dose of 6 mg-PTX per kg-body weight. At time points of 0 (pre-dose), 0.5, 1, 2, 4, 6, 8, 12, and 24 h after injection, the blood was collected and centrifuged at 6000 rpm for 8 min, followed by a liquid-liquid extraction. In a typical extraction, plasma sample (200 μL) was mixed with diethyl ether (3 mL) containing diazepam (1.0 μg mL^{-1}, 50 μL) as an internal standard. The samples were extracted in a vortex-mixer for 2 min following by a centrifugation at 3000 rpm for 10 min. The organic layer was transferred to a clean tube and evaporated under nitrogen. The extracted residue was dissolved in acetonitrile (100 μL) and centrifuged at 3000 rpm for 5 min before HPLC analysis.

Tumor Xenografts and In Vivo Imaging: HeLa tumor cells were harvested by centrifugation and re-suspension in sterile PBS. Then, the tumor cells (1×10^6 cells/site) were implanted subcutaneously into the right foreleg of female athymic nude mice (4 weeks old). Biodistribution and imaging studies were performed when the tumor size reached ≈0.5 cm (3 weeks after post-inoculation). In vivo florescence imaging was performed with a Kodak (DXS 4000 PRO system) in vivo imaging system. Florescence signals were analyzed by the Kodak Molecular Imaging Software.

Characterization Methods: TEM images were taken on a TecnaiG220 electron microscope operating at 200 kV. The number-average molecular weight (M_n), the weight-average molecular weight (M_w), and the polydispersity index (PDI) were analyzed by gel permeation chromatography (GPC). The conversion in the polymerization reaction was determined by the gravimetry. ^{1}H NMR and ^{13}C NMR analyses were performed on a UNITY INOVA 400 MHz and a Varian NMRststem-300 MHz spectrometer, respectively. Photoemission and photoexcitation spectra were recorded on an Edinburgh-920 fluorescence spectra photometer; in vivo and ex vivo images were taken using a DXS 4000 PRO system (Kodak) (λ_{ex} = 405 nm).

Supporting Information

Supporting Information is available from the Wiley Online Library or from the author.

Acknowledgements

This work was financially supported by the Ministry of Education, Singapore, under Grants R-279-000-295-133, R-279-000-327-112 and Natural Science Foundation of Jiangsu Province (BK2012625).

Received: February 1, 2013
Published online: April 11, 2013

[1] E. Boisselier, D. Astruc, *Chem. Soc. Rev.* **2009**, *38*, 1759.
[2] W. Cai, X. Chen, *Small* **2007**, *3*, 1840.
[3] R. Hao, R. Xing, Z. Xu, Y. Hou, S. Gao, S. Sun, *Adv. Mater.* **2010**, *22*, 2729.
[4] S. Balasubramanian, D. Kagan, C.-M. Hu, S. Campuzano, M. J. Lobo-Castañon, N. Lim, D. Y. Kang, M. Zimmerman, L. Zhang, J. Wang, *Angew. Chem. Int. Ed.* **2011**, *50*, 4161.
[5] H. Cheng, C. J. Kastrup, R. Ramanathan, D. J. Siegwart, M. Ma, S. R. Bogatyrev, Q. Xu, K. A. Whitehead, R. Langer, D. G. Anderson, *ACS Nano* **2010**, *4*, 625.
[6] X. Wu, T. Ming, X. Wang, P. Wang, J. Wang, J. Chen, *ACS Nano* **2010**, *4*, 113.
[7] C. M. Jewell, J. M. Jung, P. U. Atukorale, R. P. Carney, F. Stellacci, D. J. Irvine, *Angew. Chem. Int. Ed.* **2011**, *50*, 12312.
[8] X. Qian, X. H. Peng, D. O. Ansari, Q. Yin-Goen, G. Z. Chen, D. M. Shin, L. Yang, A. N. Young, M. D. Wang, S. Nie, *Nat. Biotechnol.* **2008**, *26*, 83.
[9] C. M. Cobley, J. Chen, E. C. Cho, L. V. Wang, Y. Xia, *Chem. Soc. Rev.* **2011**, *40*, 44.
[10] Y. Tang, M. Ouyang, *Nat. Mater.* **2007**, *6*, 754.
[11] I. I. Slowing, J. L. Vivero-Escoto, C.-W. Wu, V. S. Y. Lin, *Adv. Drug Delivery Rev.* **2008**, *60*, 1278.
[12] J. I. Park, A. Saffari, S. Kumar, A. Günther, E. Kumacheva, *Annu. Rev. Mater. Res.* **2010**, *40*, 415.
[13] M. Liong, J. Lu, M. Kovochich, T. Xia, S. G. Ruehm, A. E. Nel, F. Tamanoi, J. I. Zink, *ACS Nano* **2008**, *2*, 889.
[14] R. Jin, *Nanoscale* **2010**, *2*, 343.
[15] Y. Negishi, Y. Takasugi, S. Sato, H. Yao, K. Kimura, T. Tsukuda, *J. Am. Chem. Soc.* **2004**, *126*, 6518.
[16] O. M. Bakr, V. Amendola, C. M. Aikens, W. Wenseleers, R. Li, L. D. Negro, G. C. Schatz, F. Stellacci, *Angew. Chem. Int. Ed.* **2009**, *48*, 5921.
[17] L. Shang, S. Dong, G. U. Nienhaus, *Nano Today* **2011**, *6*, 401.
[18] J. Zheng, C. Zhang, R. M. Dickson, *Phys. Rev. Lett.* **2004**, *93*, 077402.
[19] J. Xie, Y. Zheng, J. Y. Ying, *J. Am. Chem. Soc.* **2009**, *131*, 888.
[20] X. Michalet, F. F. Pinaud, L. A. Bentolila, J. M. Tsay, S. Doose, J. J. Li, G. Sundaresan, A. M. Wu, S. S. Gambhir, S. Weiss, *Science* **2005**, *307*, 538.
[21] S. M. Nie, Y. Xing, G. J. Kim, J. W. Simons, *Annu. Rev. Biomed. Eng.* **2007**, *9*, 257.

[22] S. Choi, R. M. Dickson, J. Yu, *Chem. Soc. Rev.* **2012**, *41*, 1867.
[23] C. Zhou, M. Long, Y. Qin, X. Sun, J. Zheng, *Angew. Chem. Int. Ed.* **2011**, *50*, 3168.
[24] H. S. Choi, W. Liu, P. Misra, E. Tanaka, J. P. Zimmer, B. I. Ipe, M. G. Bawendi, J. V. Frangioni, *Nat. Biotechnol.* **2007**, *25*, 1165.
[25] C. Zhou, G. Hao, T. Patrick, J. Liu, M. Yu, S. Sun, O. Oz, X. Sun, J. Zheng, *Angew. Chem. Int. Ed.* **2012**, *51*, 10118.
[26] V. P. Torchilin, *Adv. Drug Delivery Rev.* **2006**, *58*, 1532.
[27] J. H. Park, S. Lee, J. H. Kim, K. Park, K. Kim, I. C. Kwon, *Prog. Polym. Sci.* **2008**, *33*, 113.
[28] C. Khemtong, C. W. Kessinger, J. Gao, *Chem. Commun.* **2009**, *24*, 3497.
[29] M. Zhao, D. A. Beauregard, L. Loizou, B. Davletov, K. M. Brindle, *Nat. Med.* **2001**, *7*, 1241.
[30] S. Laurent, D. Forge, M. Port, A. Roch, C. Robic, E. L. Vander, R. N. Muller, *Chem. Rev.* **2008**, *108*, 2064.
[31] K. Cheng, S. Peng, C. Xu, S. Sun, *J. Am. Chem. Soc.* **2009**, *131*, 10637.
[32] H. Kawaguchi, *Prog. Polym. Sci.* **2000**, *25*, 1171.
[33] S. F. M. van Dongen, H.-P. M. de Hoog, R. J. R. W. Peters, M. Nallani, R. J. M. Nolte, J. C. M. van Hest, *Chem. Rev.* **2009**, *109*, 6212.
[34] P. Debbage, *Curr. Pharm. Des.* **2009**, *15*, 153.
[35] D. Schmaljohann, *Adv. Drug Delivery Rev.* **2006**, *58*, 1655.
[36] A. K. Bajpai, S. K. Shukla, S. Bhanu, S. Kankane, *Prog. Polym. Sci.* **2008**, *33*, 1088.
[37] W. Meier, *Chem. Soc. Rev.* **2000**, *29*, 295.
[38] L. Linderoth, G. H. Peters, R. Madsen, T. L. Andresen, *Angew. Chem. Int. Ed.* **2009**, *48*, 1701.
[39] Z. Luo, X. Yuan, Y. Yu, Q. Zhang, D. T. Leong, J. Y. Lee, J. Xie, *J. Am. Chem. Soc.* **2012**, *134*, 16662.
[40] D. Chen, N. Li, H. Gu, X. Xia, Q. Xu, J. Ge, J. Lu, Y. Li, *Chem. Commun.* **2010**, *46*, 6708.
[41] Y. Zheng, S. Gao, J. Y. Ying, *Adv. Mater.* **2007**, *19*, 376.
[42] E.E. Dormidontova, *Macromolecules* **1999**, *32*, 7630.
[43] H. Maeda, J. Wu, T. Sawa, Y. Matsumura, K. Hori, *J. Controlled Release* **2000**, *65*, 271.
[44] L. Carr, G. Cheng, H. Xue, S. Jiang, *Langmuir* **2010**, *26*, 14793.
[45] C. A. Simpson, K. J. Salleng, D. E. Cliffel, D. L. Feldheim, *Nanomedicine: NBM* **2013**, *9*, 257.